ORIGINAL RESEARCH ARTICLE

Image-based sensing of salt stress in grapevine

Giuseppe Montanaro[1*], Nunzio Briglia[1], Angelo Petrozza[2], Antonio Carlomagno[1], Laura Rustioni[3], Francesco Cellini[2] and Vitale Nuzzo[1]

[1] Università degli Studi della Basilicata, Italy
[2] ALSIA Centro Ricerche Metapontum Agrobios, s.s. Jonica 106, km 448,2, Metaponto, MT 75010, Italy
[3] Department of Biological and Environmental Sciences and Technologies, University of Salento, Lecce, Italy

correspondence:
giuseppe.montanaro@unibas.it

Associate editor:
Thierry Simonneau

ABSTRACT

Grapevine is among the most economically important crops suffering environmental constraints, including drought and salt stress. Although imaging is increasingly used to detect abiotic stress in agriculture, image-based phenotyping in grapevine still needs optimisation. This study presents the RGB-(red, green, blue)-based phenotyping of the early stage of salt stress response in potted grapevine (Aleatico/SO4) irrigated with saline water (100 mM NaCl) for 9 days in contrast with vines irrigated with fresh water. The response was measured using stomatal conductance (g_s), net photosynthetic rate (A), transpiration (E), maximum potential photosynthetic efficiency (F_v/F_m), stem water potential (SWP) concurrently with RGB imaging via a robotised platform.

The image-based phenotyping of salt-stressed vines employed two sets of measurements: (*i*) the pixel fraction of specific colour bands (Yellow, Green, Brown and Dark Green) and (*ii*) the mean pixel value of R, G and B and other RGB-based colorimetric indexes. Results show that the responses of g_s, A, E, F_v/F_m were closely related to increasing soil electrical conductivity (EC) and that imaging could detect the EC threshold of approx. 4 dS m-1 causing a ~ 60 % decrease in these physiological traits compared to the pre-stress level. The SWP declined to about −0.7 MPa at the end of the experiment. The change of the relative pixel fraction of Dark Green to increasing EC has been analysed within a dose-response context, showing that a decrease of 1 % of the Dark Green colour band corresponded to the 4 dS m-1 EC threshold. This study also examined the use of the mean pixel value of the R, G and B channels as proxies of EC along with new RGB-based indexes resulting from the rearrangement of original R, G and B mean pixel values. Results show the suitability of the mean pixel value of R and Coloration Index [(R-B)/R] to serve as predictors of EC ($R^2 >= 0.80$).

INTRODUCTION

Grapevine is among the most widespread and economically important crops suffering environmental constraints such as increased levels of thermo-radiation and incidences of drought and salt stress (Keller, 2010; Amato *et al.,* 2020; Marín *et al.,* 2021). Soil salinity is increasingly threatening agriculture globally and it is predicted to impact 50 % of cultivated land by 2050 (Hu and Schmidhalter, 2023). Hence, winegrowers will increasingly face environmental constraints to the extent that saline waters (e.g., Na_2SO_4 + $MgSO_4$, NaCl) would be used as alternative water resources for irrigation in Mediterranean grapevine (Martínez-Moreno *et al.,* 2022). It is worth noting that some authors (Mirás-Avalos and Intrigliolo, 2017; Martínez-Moreno *et al.,* 2023) report minimal impacts of salty water on vine performances in the short period. Moreover, the quality of groundwater is decreasing due to salt intrusion and pollutants from various sectors (see Weerasekera, 2017). Following this, research activities improving the understanding of the salinity stress response can support identifying genetic resources and management solutions to challenging environments.

Under salinity stress, plant response generally follows a two-stage pattern. The initial stage is dominated by osmotic stress due to increased salt concentration in the soil (Isayenkov and Maathuis, 2019), while the concentration of critical ions (e.g., Na^+) in the leaf remains unchanged. Thereafter, with persistent salinity stress, plants accumulate a toxic level of these ions in the older leaves and shoots, causing necrosis and premature canopy senescence (Munns and Tester, 2008).

The initial (leaf) ion-independent response to salt stress is increasingly attracting interest in research studies focussing on the physiological limitations induced by salt accumulation into the soil, even though leaves do not accumulate ions above the non-stressed level. For example, in grapevine, initial exposure to salinity triggered both stomatal and metabolic impairments of photosynthesis and, in turn, reduced shoot growth while ion concentrations in leaves remained comparable to that of control (Montanaro *et al.,* 2022). The above-mentioned stomatal closure is a common response to initial salt stress and it conceivably determines the reduction of transpiring flux to reduce the rate of water uptake and thus of salts (Munns and Tester, 2008). In addition, improving understanding of the early response to salinity stress response would support the screening of plant populations for tolerant individuals. For example, Atieno *et al.* (2017) explored the genetic variation for salinity tolerance in chickpeas under ion-independent stress.

Nowadays, plant stress recognition is increasingly pursued through high-throughput plant phenotyping as an innovative, non-invasive, image-based technology. In line with this, the response of grapevine to environmental constraints (e.g., drought, pathogens) has recently been the subject of studies employing image-based datasets in which different parts of the plant (e.g., whole canopies or single leaves) are interrogated through different image-acquisition systems (e.g., from drones or robotised platforms) (Briglia *et al.,* 2019 and 2020; Ouyang *et al.,* 2021). Particularly, red, green and blue (RGB) colour bands and related colorimetric indexes (e.g., Dark Green) have been revealed as promising digital proxies of drought stress also because RGB cameras are easily accessible even through smartphones (Reynolds *et al.,* 2018; Ninomiya, 2022). However, image-based phenotyping of grapevines subjected to salt stress has not received much attention. Although various management approaches have been developed to face soil salinity (e.g., surface flashing, drip irrigation, mechanical removal of salts surface crust, use of organic soil amendments, introduction of tolerant plants, priming) (see for review Panagea *et al.,* 2016), digital tools for reliable and real-time monitoring of salt-stress need to be developed to determine plant adaptation capacity and support new breeding strategies (Costa *et al.,* 2019). Moreover, a digital tool might support the scoring of symptoms of salt injury, which are often based on human visual assessment (e.g., Doulati Baneh *et al.,* 2014). Hence, additional knowledge on smart plant phenotyping in grapevine under salinity stress would create the basis for an early assessment of that stress, identifying digital proxies of traits enabling the transition toward digital agriculture. In plant phenotyping, a method to build up a dose–response curve has been proposed accounting for traits related to leaf mass (or leaf area) (Poorter *et al.,* 2010). However, to the best of our knowledge, till now, a dose–response curve has not been used to describe the response of an image-based colorimetric trait to soil salinity.

This study aimed to test the hypothesis that RGB-based imaging technology can parametrise the early response to salt stress in grapevine. To test this hypothesis, gas exchanges, fluorescence and stem water potential, leaf ions and pigments were analysed in grapevines (Aleatico/SO4) irrigated with saline water (100 mM NaCl) along with RGB images pictured at a robotises phenotyping platform.

MATERIALS AND METHODS

1. Plant material and experimental design

The experiment was conducted at the ALSIA-CRMA research centre in Southern Italy (40°23'31.4''N, 16°47'10.9''E). We used grapevines (*Vitis vinifera* L) cv. Aleatico grafted onto SO4 rootstocks (*Vitis berlandieri* Planch × *Vitis riparia* Michx) growing in a greenhouse. Vines were two years old, with a single (~ 1 m) vertical leafy shoot of current season growth. Vines were grown in 3.5 L PVC pots. The growth substrate was a 3:1 v/v mixture of sandy loam soil (82 % sand, 7 % silt and 11 % clay) and peat. Plants were fertilised 15 days before the experiment using 3 g per pot of NPK fertiliser 14.7.14 (Slowenne 212, Valagro Spa, Atessa, Italy). Vines were irrigated daily (about 19 h) using tap water (57 mg/L Ca^{+2}, 1 mg/L K^+, 13 mg/L Mg^{+2}, 9 mg/L Na^+, 9 mg/L SO_4^{-2}, 13 mg/L Cl^-) to restore 100 % of daily water consumption and maintain soil moisture at field capacity.

For the various sampling and physiological measurements, the vine canopy was partitioned into lower (nodes 1–5 from

the base of the current season's growth), middle (nodes 6–11) and upper (nodes > 11) regions of a plant canopy according to Briglia *et al.* (2020). Several vines were prepared as above and a group of them (n = 28) was selected for uniformity and randomly assigned to a salt-stressed (SALT) or control (CTRL) group. On 17 July 2019 (Day 0), SALT vines (n = 14) were irrigated with a salt solution comprising tap water and NaCl at concentrations of 50 mM, 75 mM (Day 1) and 100 mM from Day 2 to Day 9. The CTRL vines (n = 14) did not receive salt and served as the control.

Throughout the experiment, air temperature (°C) and relative humidity (%) (HUMITER 50Y, Vaisala, Helsinki, Finland) and PAR (PPFD, µmol m^{-2} s^{-1}) (quantum sensor Model SKP 215, Skye Instruments LTD, Llandrindod, Wells, UK) were measured inside the greenhouse at 15 min intervals and hourly averages were recorded (CR200, Campbell Scientific Inc., Utah, USA). The air vapour pressure deficit (*VPD*) was later calculated from the records of air temperature and relative humidity, according to Goudriaan and van Laar (1994).

2. Soil electrical conductivity, leaf water potential, gas exchange, fluorescence and leaf ion and pigment concentration analysis

Soil electrical conductivity (EC, dS m^{-1}) was measured in each pot concurrently with leaf gas exchange measurements (see below) using a single channel meter equipped with a TDR-based probe (W.E.T. sensor, Delta-T, Devices, Cambridge, UK). Stem water potential (SWP, MPa) was measured using a Scholander-type pressure chamber (Model 600, PMS Instruments, Corvallis, OR), pressurised with nitrogen, according to the protocol by Turner (1981) and Choné *et al.* (2001). Briefly, for SWP determination, one fully expanded leaf per vine (×3 vines per treatment) was tagged on the middle region of the main shoot. The still-attached leaf was then covered with aluminium foil for at least 180 minutes before SWP measurement. The leaf was then sealed in a plastic bag, detached and promptly pressurised in the pressure chamber and the balance pressure was recorded.

Net photosynthetic rate (A, µmol CO$_2$ m^{-2} s^{-1}), stomatal conductance (g_s, mol H$_2$O m^{-2} s^{-1}) and transpiration rate (E, mmol H$_2$O m^{-2} s^{-1}) per unit leaf area were measured around midday (from 11:30 to 12:30 h) on days 0, 1, 2, 3, 6 and 9 using a portable photosynthesis system Li-Cor 6400 (Li-Cor, Inc., Lincoln, NE, USA). During gas exchange measurements, the reference CO$_2$ concentration inside the cuvette was set to the prevailing environmental condition (390 ppm) and the blocking temperature was, on average 34 °C. The PAR inside the cuvette was fixed at 900 µmol m^{-2} s^{-1} (10 % blue light) and the operating flow rate at 500 µmol s^{-1}. Gas exchange measurements were carried out on three vines per treatment using two fully expanded leaves per vine; these were selected from the mid-region of the vine. Three records per leaf were saved.

Concurrently with gas exchange measurements and on the same leaves (one reading per leaf), the maximum potential quantum efficiency of Photosystem II (F_v/F_m) was measured using a portable chlorophyll fluorometer (FluorPen FP 100, Photon Systems Instruments, Drasov, Czech Republic). A one-hour dark-adaptation was ensured before measurement using the FluorPen leaf clips.

On the last day of salinity stress (Day 9), leaves were sampled from the top, middle and bottom parts of the shoots from three vines per treatment and analysed for potassium and sodium concentrations (ICP 4200 MP-AES, Agilent Technologies, 5301 Stevens Creek Blvd. Santa Clara, CA 95051, US) reported as mass per unit of dry weight. After the SWP measurements, two disks per leaf (each 6.16 cm²) were excised and stored (–80 °C) for chlorophyll (Chl) and total carotenoids (xanthophyll plus carotenes) determination.

(a)   (b)
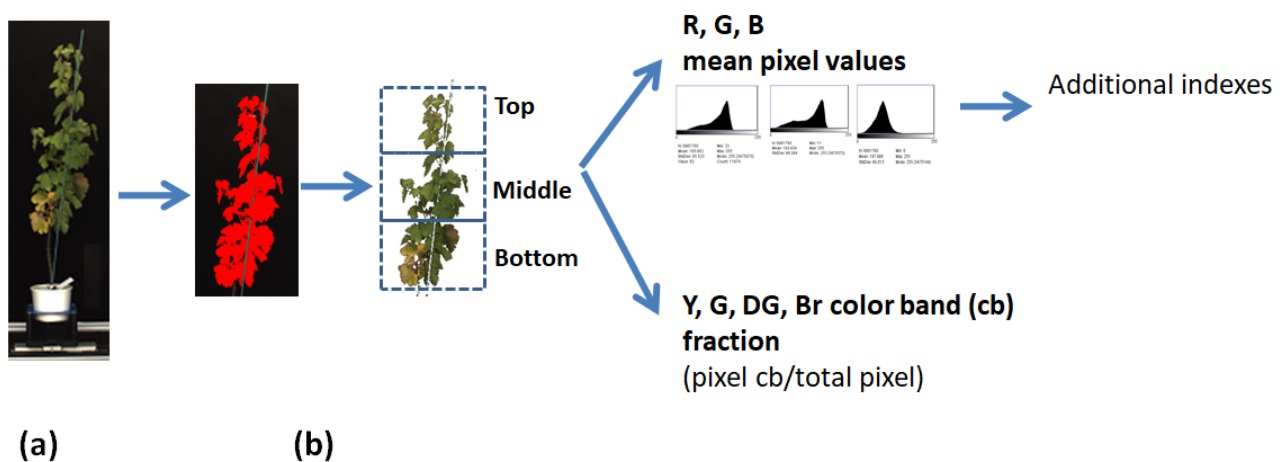
FIGURE 1. Schematic workflow of image segmentation and data analysis: after the picture acquisition (a) and segmentation (b), the three regions of interest (ROI) (top, middle, bottom) were identified. Thereafter, for each ROI, the mean pixel values of red (R), green (G) and blue (B) were determined. On each ROI, the fraction of the yellow (Y), G, dark green (DG) and brown (Br) were determined as the ratio between the number of pixels falling in the specific colour band and the total number of pixels.

Each frozen disk was separately crushed under liquid N_2 and the powder was extracted with 10 mL EtOH for 24 h at room temperature (*c*. 20 °C). Absorbances of the supernatant were determined spectrophotometrically (Varian 50-BIO, Varian Australia Pty Ltd, Victoria 3170 Australia) at 470, 649 and 665 nm and the amounts of Chl-*a*, Chl-*b* and carotenoids calculated according to Lichtenthaler and Wellburn (1983).

3. RGB imaging

A group of five vines per treatment was imaged around midday (from 12:00-13:00 h) on days 0 (just before salt treatment was initiated), 1, 2, 3, 6 and 9 using a LemnaTec 3D Scanalyzer phenotyping platform (LemnaTec GmbH, Aachen, Germany). The platform is located at the ALSIA-CRMA laboratories, part of the European Plant Phenotyping Network and infrastructures (https://emphasis.plant-phenotyping.eu/about). Vines were automatically conveyed into the imaging chamber for image acquisition. The chamber for the RGB image was equipped with two visible light cameras (2 Mpixel, Basler Scout scA1600-28gc, Colour, 1624 × 1234 pixels, ICX274 1/1.8" CCD, 28 fps, C Mount, Gigabit Ethernet). The lighting inside the chamber employed fluorescent tubes Osram T5FH 21 W 865 HE. Two images were acquired for each vine, one from each lateral orthogonal direction (0° and 90°). The image segmentation and analyses were carried out using the software LemnaGrid v5 following Arvidsson *et al.* (2011). For the image analysis, according to Briglia *et al.* (2020), the vine canopy was partitioned into the following regions of interest: bottom (nodes 1–5 from the base of the current season's growth), middle (nodes 6–11) and top (nodes > 11). For each region of interest, the LemnaGrid software v5 (LemnaTec GmbHc,

Germany) operated a colour classification of the RGB images in Dark Green, Green, Yellow and Brown colour classes according to Acosta-Gamboa *et al.* (2017). Details on the RGB reference values (anchor points) per colour class are reported by Briglia *et al.* (2019). The mean pixel values of R, G and B were also determined. Additional RGB-based indexes were also determined according to Montanaro *et al.* (2023). A schematic workflow of the image segmentation and analysis is reported in Figure 1.

4. Data analysis

Data processing and curve fitting employed OriginPro 9.1.0 (OriginLab Corporation, Northampton, MA 01060 USA). A one-way ANOVA or Kruskal–Wallis' test was used to examine the differences between treatments and the Duncan test as a post-hoc test for multiple comparisons, *p*-values < 0.05 were considered significant. The function to fit the EC vs Dark Green colour band fraction and the threshold EC (EC*t*) were determined according to Martínez-Cob *et al.* (1987).

RESULTS

This study reports physiological and phenotypic changes induced by a 10-day salt stress, causing an increase in soil EC up to about 8 dS m^{-1} (Figure 2). At the end of the experiment, leaves from the bottom, middle and top regions of the main stem in salt-stressed vines showed concentrations of K^+ and Na^+ comparable to those in CTRL vines (Figure 3). In contrast to this, the mean concentration of the Chl-*a* was significantly reduced by the salt stress
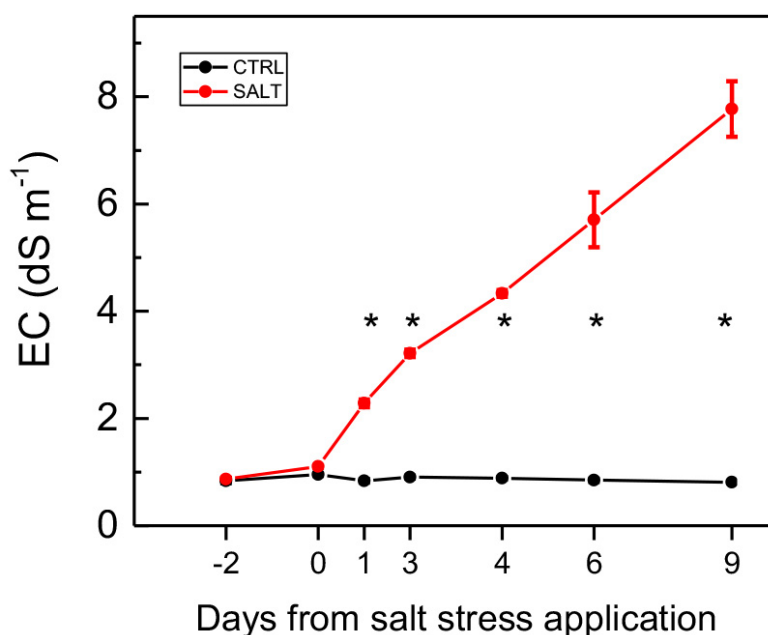
FIGURE 2. Variations in soil electrical conductivity in control (CTRL) salt-stressed (SALT) vines.

Comparing treatments at the same time, * indicates statistically significant differences (*p* < 0.05). Values are mean ±SE (n = 14) and are visible only when larger than the symbol.
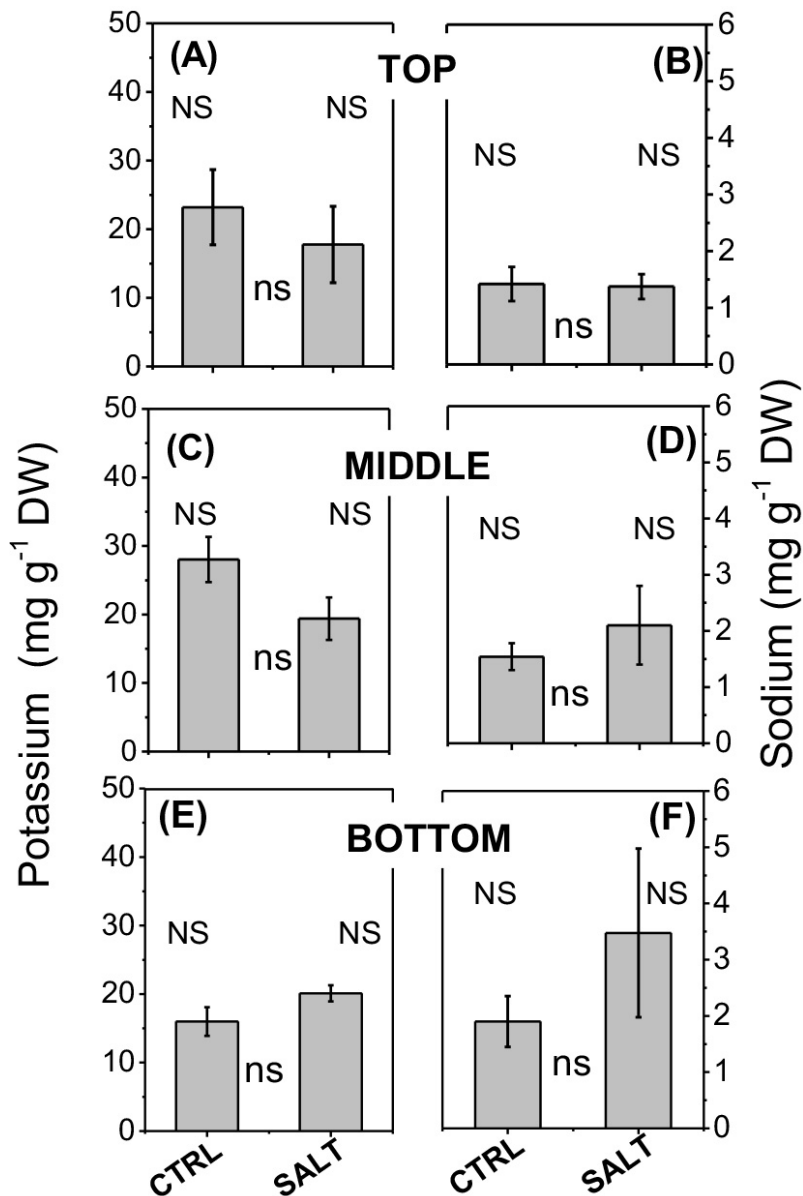
FIGURE 3. Concentrations of (A, C, E) potassium and (B, D, F) sodium detected in leaves of control (CTRL) and salt (100 mM NaCl) stressed (SALT) vines sampled on the last day (Day 9 after the salinity stress imposition) from the top, middle and bottom regions of the vine. Values are means ±SE (n = 3). NS = not-significant difference comparing regions (Top, Middle, Bottom) within the same mineral element and treatment (CTRL or SALT); ns = not-significant difference comparing treatments within the same mineral element and canopy region. Tests were carried out at α = 0.05 (Kruskal–Wallis' test).

being approx. 0.68 ± 0.04 mg g^{-1} DW, while it was approx. 1.06 ± 0.05 mg g^{-1} DW in CTRL vines (Figure 4). Similarly, the concentration of carotenoids was significantly lower than that in CTRL vines, being about 0.48 ± 0.06 mg g^{-1} DW; on the contrary, the Chl-*b* concentration did not show significant variation (Figure 4).

1. Physiological traits

The response of leaf gas exchanges to salt stress is presented in Figure 5. Results show that g_s in CTRL vines was roughly stable during the experiment after an initial decline to

0.15–0.18 mol m^{-2} s^{-1} detected on Day 3, likely due to a declined *VPD* (Figure 6). Contrary to this, as early as the day after the salt application, stomatal conductance (g_s) declined to about 0.15 ± 0.01 mol m^{-2} s^{-1} while it was at about 0.25 ± 0.01 mol m^{-2} s^{-1} in CTRL vines (Figure 5A). Thereafter, g_s continued to decline, reaching $0.013 \pm 8.1 \times 10^{-4}$ mol m^{-2} s^{-1} on Day 9 after the start of salt application (Figure 5A).

Stomatal limitations of gas exchanges induced by salt stress significantly influenced transpiration and photosynthetic rates. Starting from Day 1 after salt imposition, transpiration
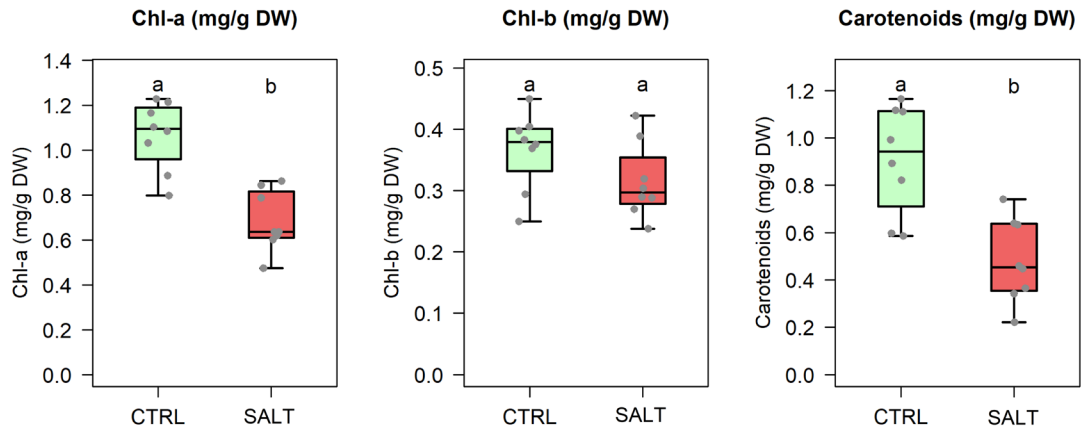
FIGURE 4. Boxplot of the concentration of (left) chlorophyll-*a*, (middle) chlorophyll-*b* and (right) carotenoids measured at the end of the experiment in leaves of vines irrigated with (CTRL) fresh and (SALT) salty water. The grey dots represent the single analytical determinations. Comparing treatments within the same pigment, the different letter indicates significant differences (Kruskal–Wallis' test, $p < 0.05$).
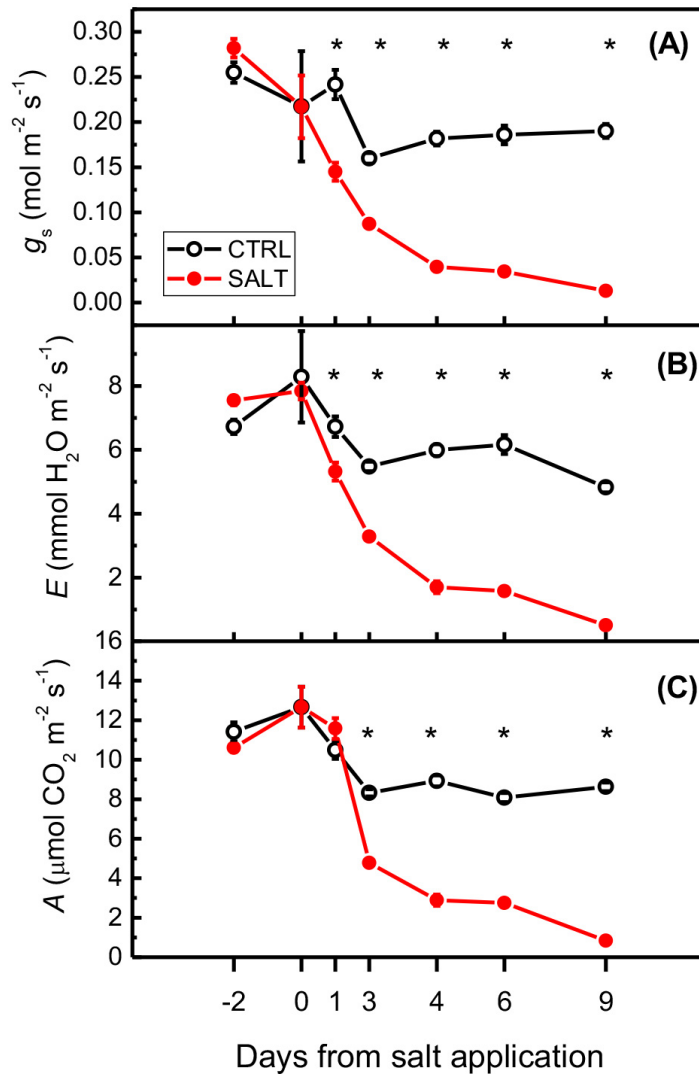

FIGURE 5. Variations in (A) stomatal conductance, (B) transpiration and (C) photosynthetic rate measured in control (CTRL, black line) and salt-stressed (SALT, red line) vines. Comparing treatments at the same time, * indicates statistically significant differences ($p < 0.05$). Values are mean ($n = 18$) ± SE and are visible only when larger than the symbol.
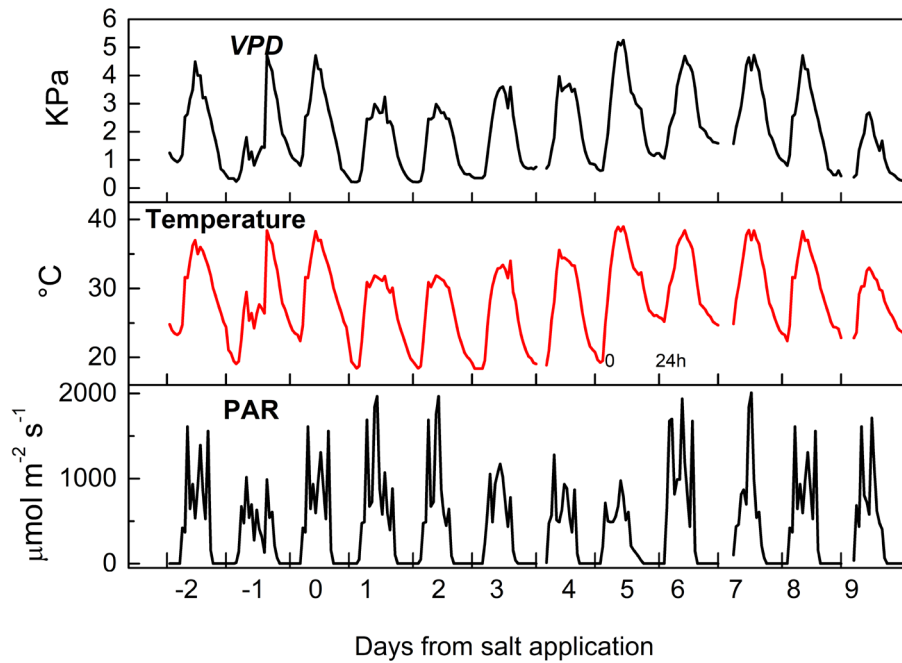
FIGURE 6. Daily course of vapour pressure deficit (*VPD*), air temperature (°C) and photosynthetically active radiation (PAR) measured in the greenhouse during the experiment.
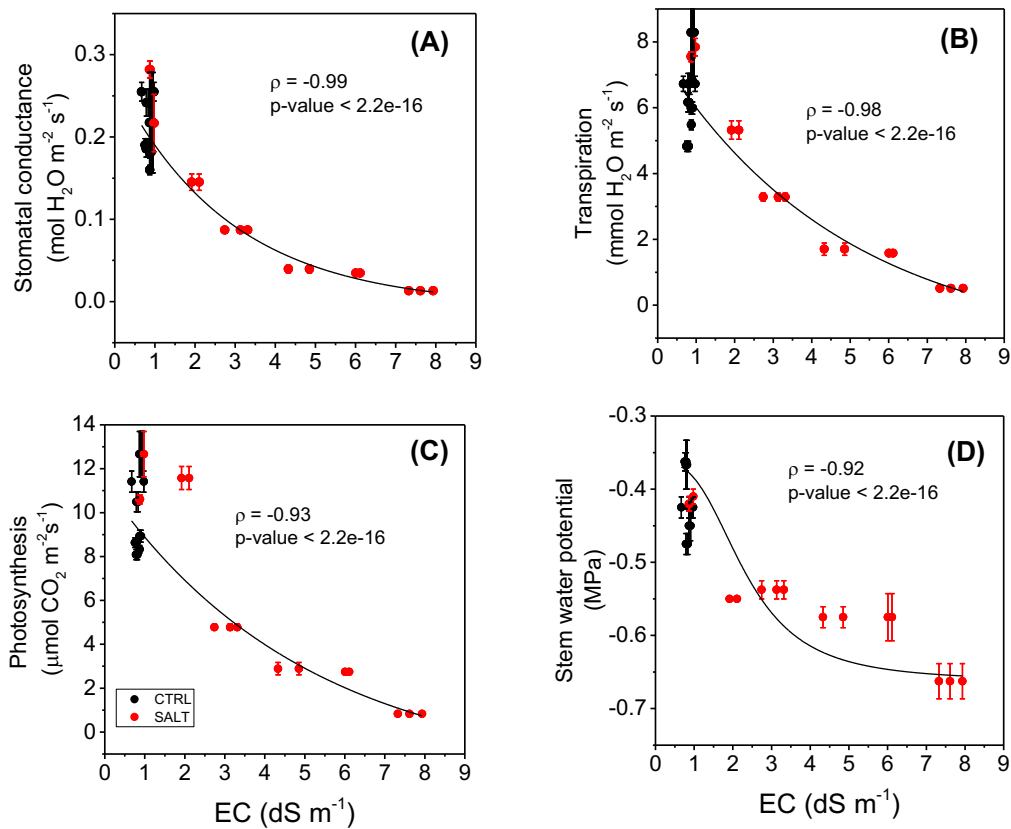
FIGURE 7. Relationship between soil electrical conductivity (EC, dS m^{-1}) and (A) stomatal conductance, (B) transpiration, (C) net photosynthetic rate and (D) stem water potential measured in control vines (CTRL, black dots) and salt-stressed vines (SALT, red dots). Valued are mean (n = 18) ± SE and are visible when larger than the symbol. All data were pooled in each panel before determining the Spearman rank correlation test (ρ) and exponential decay fitting.
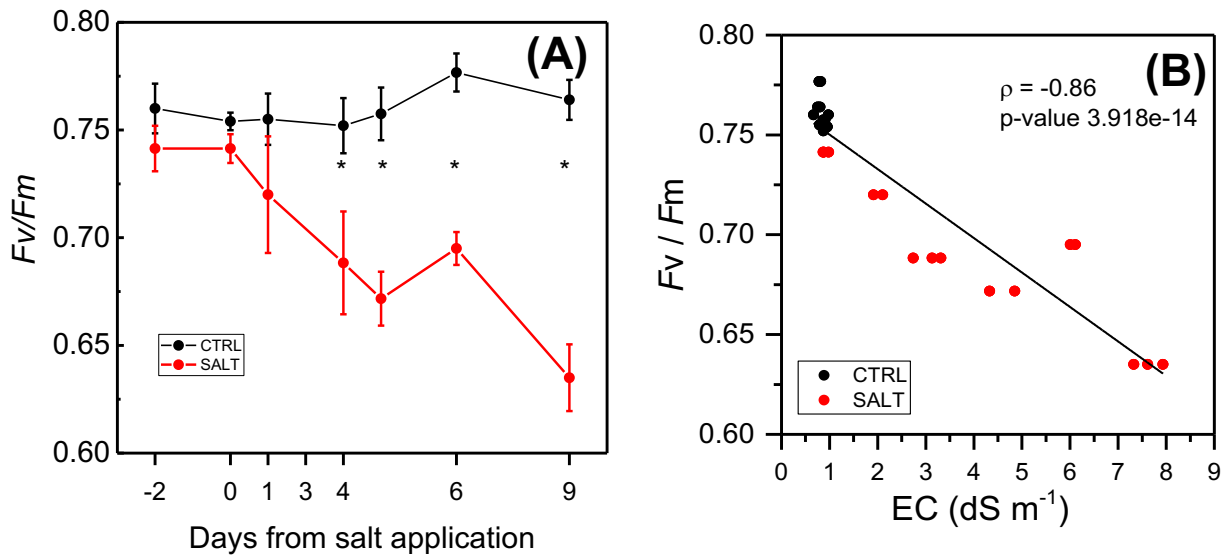
FIGURE 8. (A) Variation in chlorophyll-*a* fluorescence (F_v/F_m) measured in vines irrigated with tap water (CTRL) and under salt stress (SALT). Comparing treatments at the same time, * indicates statistically significant differences ($p < 0.05$). Values are mean (n = 6) ±SE. (B) Correlation between soil electrical conductivity (EC, dS m-1) and the Fv/Fm measured during the experiment; data were pooled before determining the Spearman rank correlation test (ρ) and linear fitting.

rate (E) in salt-stressed vines progressively declined, reaching about 1.7 ± 0.18 mmol H_2O m^{-2} s^{-1} on Day 4 (Figure 5B). Thereafter, E further declined, reaching an average value of 0.51 ±0.03 mmol H_2O m^{-2} s^{-1} at the end of the experiment. Similarly, the net assimilation rate (A) in stressed vines steeply declined from the mean value of ~ 12.6 ±1.03 μmol CO_2 m^{-2} s^{-1} (Day 0) to around 4.78 ±0.14 μmol CO_2 m^{-2} s^{-1} on Day-3 (Figure 5C). During the following days, the mean value of A continued to progressively decline towards the minimum of 0.83 ± 0.06 μmol CO_2 m^{-2} s^{-1} at the end of the experiment (Figure 5C).

The physiological parameters examined (A, E and g_s) declined smoothly with the increasing EC and were (negatively) significantly correlated with EC, showing the Spearman rank test (rho, ρ) ranging from –0.92 to –0.99 (Figure 7A–C). Similarly, the stem water potential (SWP) declined with increasing soil EC (Figure 7D). However, after an initial prompt decline recorded at soil EC values of about 2 dS m^{-1}, the SWP remained stable at approx. –0.55 MPa despite the increasing soil EC up to 6 dS m^{-1}. Values of EC beyond ~6 dS m^{-1} further decreased the SWP (Figure 7D).

The maximum potential photosynthetic efficiency (F_v/F_m) in CTRL vines was, on average, ~0.76 throughout the experiment, whereas in leaves under salt stress, it significantly declined to ~0.63 (Day 9) if a transient increase recorded on Day 6 is excepted (Figure 8A).

During the salt stress period, the soil EC (Figure 2) progressively increased from about 0.80 dS m^{-1} (starting point) to about 8.0 dS m^{-1} by the end of the trial, whereas it

remained almost stable at around 0.75 dS m^{-1} in CTRL vines. Similarly to gas exchanges, the F_v/F_m showed a significant negative correlation (ρ = -0.86) with the increasing soil EC (Figure 8B).

2. Image-based salt-stress phenotyping

In our study, RGB images have been employed for phenotyping the effects of salt stress through analysis of variations in mean pixel values of R, G and B and in other RGB-based colorimetric indexes. At the end of salt stress, the bottom leaves of vines had visible colour changes, while the middle and top ones remained visually comparable to those in CTRL (Figure 9).

The map of the colour band fractions determined across the salt stress period is reported in Figure 9. The Dark Green was the most prominent colour band, allowing easy recognition of its variation. From Day 3, after salt stress imposition, the bottom region of salt-stressed vines showed a significant reduction of the Dark Green fraction compared to CTRL ones, reaching a significant ~43 % lower value on Day 9 (Figure 9). The fraction of the Brown colour band (bottom region) in CTRL vines was stably about 5 % throughout the experiment, while it significantly increased in salt-stressed ones, reaching 14 % and 38 % on Day 6 and Day 9, respectively (Figure 9).

The response of Dark Green was correlated to increasing soil EC, showing a high coefficient of determination (R^2) equal to 0.71 and 0.73 in the middle and bottom regions, respectively (Figure 10). In addition, the EC value of 4.2 dS m^{-1} was
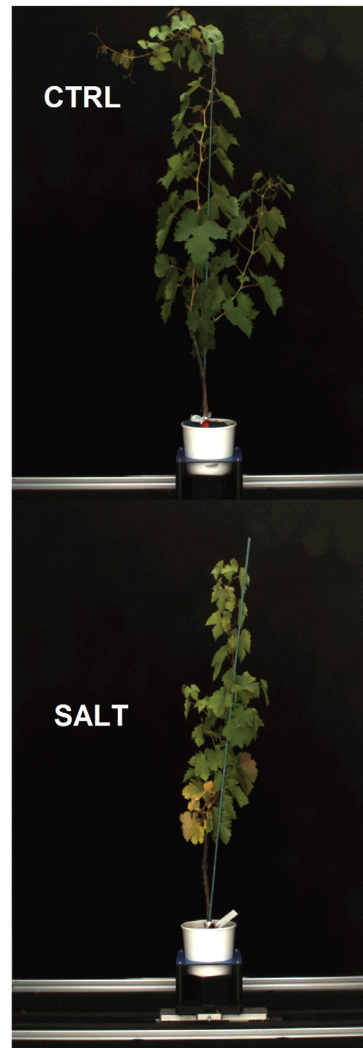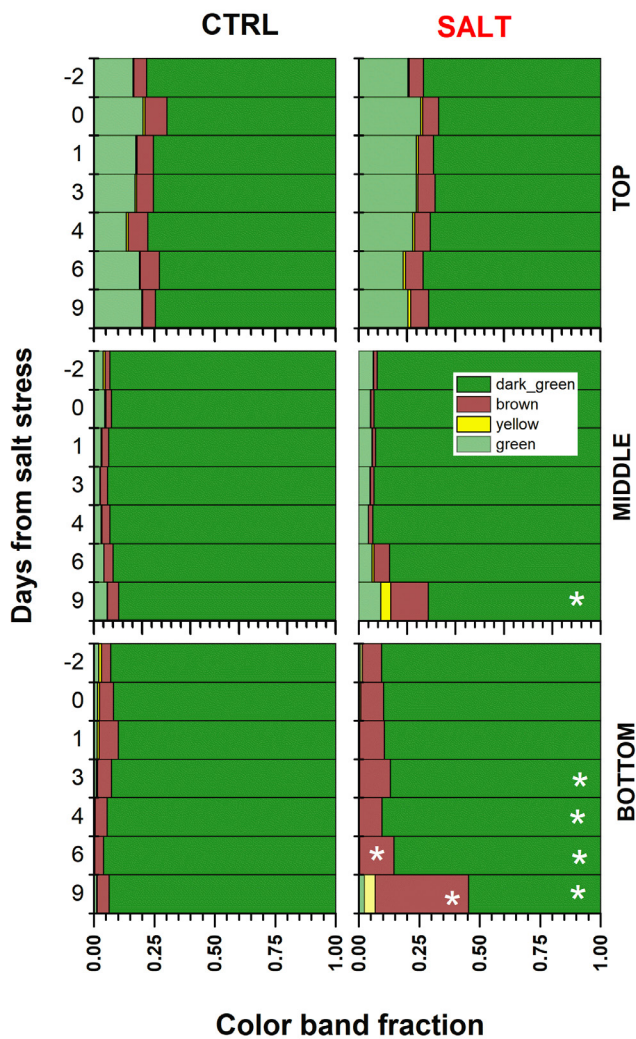
FIGURE 9. Left: map of the fraction of the colour bands observed during the experiment in control (CTRL), left column) and salt-stressed (SALT, right column). Data refer to the Top, Middle and Bottom regions of the vines, comparing treatments within the same day and colour band fraction, * indicates significant differences ($p < 0.05$). Right: phenotypic variation of grapevine irrigated with fresh water (CTRL) and exposed to salt stress (SALT); RGB image of each vine has been pictured separately from each other, then they were composed for illustrative purposes. Salt stress caused leaf discolouration (mainly at the bottom region of the canopy) compared to control vines; salt also stunted growth. Due to the size of the RGB chamber, the newly growing apical shoots in the CTRL vine were not secured to the woody supporting pole, preventing them from being cut out from the frame.
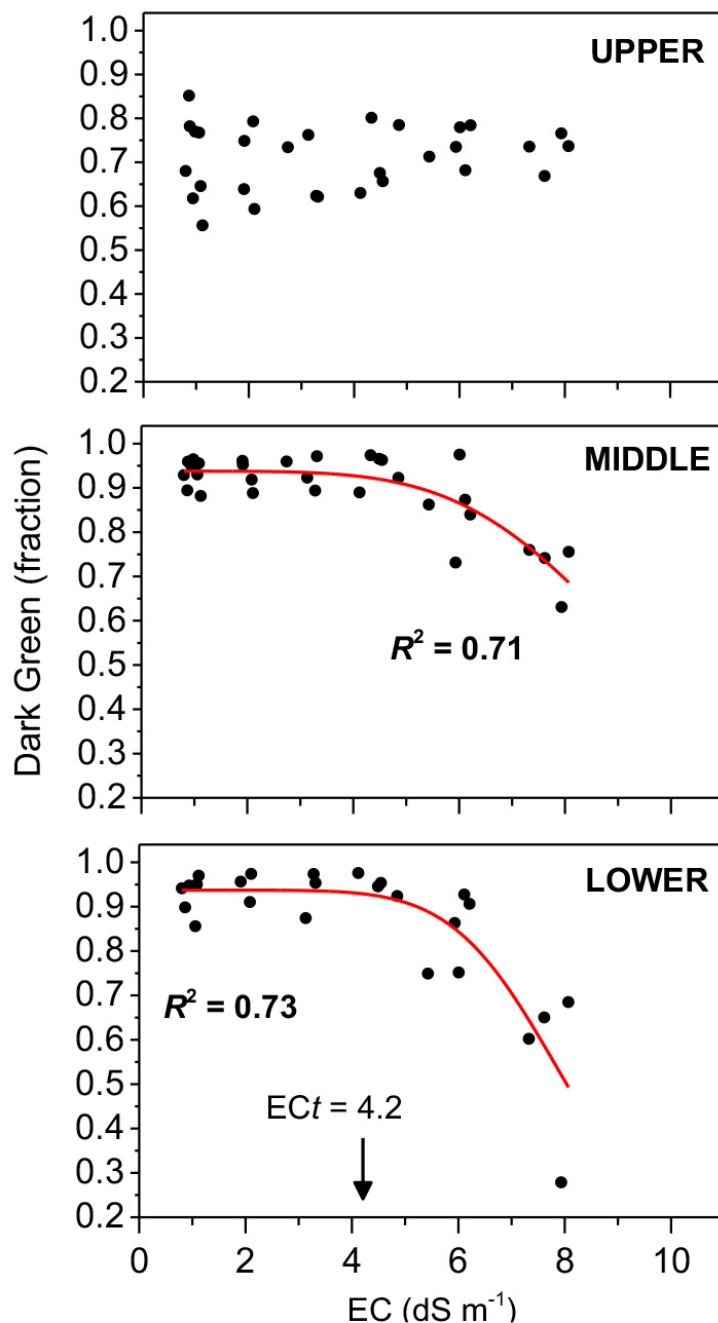
FIGURE 10. Correlation between soil electrical conductivity (EC) and Dark Green fraction measured in vines under increasing salt stress conditions. The non-linear fitting curve employed the function $Y=Y_m/[1+(EC/EC_{50})^p]$, where Y is the Dark Green fraction calculated at EC = x, Y_m is the maximum asymptote of the Dark Green fraction when soil EC=0, p is the slope at the steepest part of the curve, EC_{50} is the value of the EC when Dark Green fraction equals 50 % of Ym. Fitting lines were drawn when $p < 0.05$. The arrow indicates the threshold value of EC (ECt) corresponding to a ~1 % decline of Dark Green (Ym) measured at the lower part of the vine.

(A)   **RGB-based colorimetric indexes**

(B)

EC (dS/m)
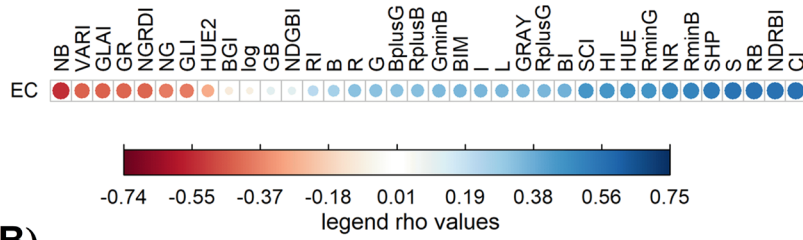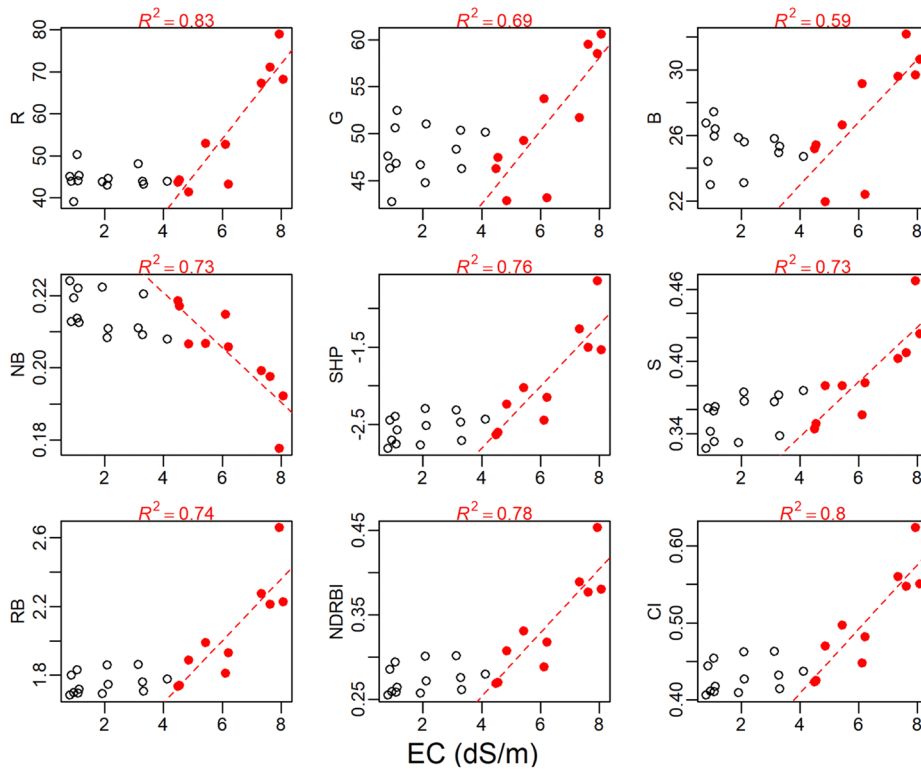
FIGURE 11. (A) Heat-map of the Spearman's rank test employed to measure the correlation between soil electrical conductivity (EC) and R, G, B and the various RGB-based colorimetric indexes measured in the bottom part of the canopy in salt-stressed vines. Note that the variables have been sorted according to ascending ρ values from the minimum –0.74 (NB, Normalised Blue) to the maximum 0.75 (CI, Colouration Index) and that the legend scale has been drawn within the same range. (B) Scatterplot between soil EC and R, G, B and some RGB-based colorimetric indexes measured in salt-stressed vines. Note that solid symbols refer to paired values measured at EC > 4.2 dS m-1 (see Figure 10 for details on the EC threshold). The values of the coefficient of determination (R2) refer to a linear model Y ~ a*x +b, where the x was the EC data belonging to solid points, Y was the colorimetric variable and a and b were the slope and the Y-axis intercept, respectively. For full details on the colorimetric index, see Montanaro *et al.*, 2023.

determined as a threshold value corresponding to the change of 1 % of the maximum value of the fitting model of the Dark Green in the bottom region.

Increasing soil EC had an erratic covariation with the mean pixel values of the R, G, B and RGB-based indexes to the extent that the Spearman's rank test (rho, ρ) ranged from –0.74 to 0.75 (Figure 11A). For those colorimetric variables having a high ρ, we had a roughly good linear correlation with EC values detected at EC > 4.2 dS m^{-1} (Figure 11B). For example, in the case of R and CI indexes, the values of R^2 were considerably >= 0.8 (Figure 11B).

DISCUSSION

The present study reports on image-based proximal sensing of salt stress in grapevine employing RGB images, focussing on the early stage of the stress, which is independent of the toxic accumulation of ions (Munns and Tester, 2008). Accordingly, the critical ion (i.e., Na^+) did not accumulate above the control level in the salt-stressed leaves; additionally, it was approx. 15–30 % of those reported in a 10-day (Mohammadkhani and Abbaspour, 2017) and 2-week (Fozouni *et al.,* 2012) salt exposure. Similarly, the concentration of K^+ was not influenced by salt stress and was consistent with that reported in Amorim *et al.* (2023) for the same SO4 rootstock after two weeks of salt stress. The unincreased leaf concentration of K^+ and Na^+ in stressed vines supports this in the early (osmotic) stage of salt stress (Munns and Tester, 2008). Although the significance of treatments (CTRL, SALT) and vine region (Top, Middle, Bottom) was appropriately evaluated using a non-parametric test (Kruskall–Wallis), the number of chemical analyses for K^+ and Na^+ should be increased to improve the robustness of the comparison.

In this study, we did not check for Cl^- accumulation as Na^+ is the most prominent factor causing damage in grapevines under salt stress (Dag *et al.,* 2015). Moreover, the role of Cl^- in causing salt-related impairments (e.g., photosynthesis decline) remains controversial (Baggett *et al.,* 2021). Despite correlative information on paired accumulation of Na^+ and Cl^- are available also showing similar increases (Walker *et al.,* 1997; Meggio *et al.,* 2014), measuring the concentration of Cl^- in response to the osmotic stage of salt stress would provide a more complete picture.

Although we found no significant change in leaf Na^+ and K^+ concentrations, salt stress caused several physiological responses. That is, soon after salty water application values in maximum potential quantum efficiency of Photosystem II (F_v/F_m) as well as in the other examined leaf functional traits (A, E and g_s) showed a prompt deviation of about 9 % (F_v/F_m), 40 % (A, g_s) and 15 % (E) from those recorded in CTRL vines.

Clearly, stomatal and metabolic impairments of photosynthesis occurred within a few days after salt stress application, confirming the sensitivity of *Vitis spp.* to salt exposure (Maas and Hoffman, 1977; Prior *et al.,* 1992; Cramer *et al.,*

2006; Meggio *et al.,* 2014) and that they were uncoupled from colour-based changes in phenotype. Following this, it could be noted that approx. 50 % reduction of the pre-stress level of gas exchange parameters and F_v/F_m occurred when soil EC approached about 4 dS m^{-1} (Figure 7,8B), whilst colour-based traits were still comparable to those in CTRL (Figure 9). Similarly, Upadhyay *et al.* (2018) reported a time lag between the impairment of key physiological parameters, including gas exchanges and the onset of visual symptoms. Hence, image-based phenotyping protocols should combine proxies based on physiological parameters (e.g., F_v/F_m) which quickly respond to salt stress. The impact of early salt stress on growing parameters (e.g., plant size, internode elongation) has been recognised in various species, including chickpea and grapevine (Atieno *et al.,* 2017; Upadhyay *et al.,* 2018; Montanaro *et al.,* 2022).

The present study was conducted on potted vines embedding some potential divergences from field experiments. However, the response of EC to salty water application is comparable to that recorded in a field experiment in a commercial vineyard (Ben-Asher *et al.,* 2006), including the following effect on SWP (Yu and Kurtural, 2020).

In our study, the image-based phenotyping of the salt-stressed vines employed two sets of measurements: (*i*) the pixel fraction of specific colour bands (Yellow, Green, Brown and Dark Green) and (*ii*) the mean pixel value of R, G and B and other RGB-based colorimetric indexes. The choice of colour bands employed to feed the LemnaGrid clustering algorithm to differentiate and calculate the relative colour classification was based on own previous research on drought stress (Briglia *et al.,* 2019), considering its similarity with the initial stage of salt stress. In addition, leaf yellowish and browning were also associated with salt stress in a salt responsive transcriptome analysis of grapevine (Das and Majumder, 2018).

Among the specific colour bands examined, results show that the pixel fractions of the Dark Green at the lower and middle regions of the vines were the most prominent and informative on the progress of the salt stress. The present study did not test whether the Dark Green fraction (or other colorimetric indices) is specific to (early) salt stress or common to all osmotic stresses. However, it was found that the variation in the Dark Green fraction within a dose-response context occurred as early as three days after salt imposition, suggesting its suitability for the detection of that stress. In Briglia *et al.* (2019), Dark Green was the best predictor of SWP in a drought stress experiment, which is in favour of its potential suitability as a predictor in both early salt and drought stress, but this remains to be specifically tested.

The upper region of the vine shoot (the youngest region) was less informative, likely because of the dichromatism of young (copper-coloured) leaves in the cultivar we tested, as it was pointed out in a drought-related study (Briglia *et al.,* 2020). Moreover, to prevent a misinterpretation of the effect of the stress caused by that dichromatism, top-view images were not considered, and only two side-view images

(at 90° from each other) were employed to capture colour-based phenotypic traits according to phenotyping studies in grapevine (Briglia *et al.,* 2019) and other crops (Klukas *et al.,* 2014; Hairmansis *et al.,* 2014; Petrozza *et al.,* 2014). Hence, considering that the colour of young leaves is a cultivar-dependent trait (see, for example, code 051 in OIV, 2009), it is advisable not to capture young leaves within the image frame, thus avoiding misinterpretation.

Following this, the response of the Dark Green pixel fraction to increasing exposure to salt was evaluated separately in each plant region, showing a close correlation with soil EC (Figure 10). Data on the Dark Green fraction were then fitted through a dose-response curve belonging to Hill functions, which are useful functions for retrieving the threshold value at which the response variable is halfway between the minimum and maximum responses (Khan *et al.,* 2003; Gadagkar and Call, 2015). The sigmoidal dose-response type equations have been employed in various contexts (Gadagkar and Call, 2015; Xue *et al.,* 2017), including the responses of seedling growth to saline conditions in barley and maise (Khan *et al.,* 2003; Xue *et al.,* 2017).

The threshold value of EC (ECt) corresponding to the initial decline (~ 1 % of maximum) of the response variable has been considered a reliable parameter for comparing various levels of salt tolerance (Martínez-Cob *et al.,* 1987). In line with this idea, it should be noted that the relative 50-60 % adaptive reduction in some gas exchange parameters in response to the salt stress occurred when soil EC approached the ECt threshold (Figure 10). However, values of ECt, as well as the relationships between colorimetric indicators and salt stress intensity (Figure 11), need to be parametrised in relation to factors affecting vine sensitivity to early (osmotic) salt stress, such as genetic diversity. For example, an *in vitro* study tested up to 40 grapevine rootstock accessions for osmotic-stress tolerance, confirming that genetic diversity induces a different morphometric response (Peiró *et al.,* 2020). Hence, the influence of the genetic diversity of rootstock (and cultivar) on RGB-based colorimetric indexes remains to be examined.

Considering that similar leaf concentrations of K^+ and Na^+ were present among the treatments (Figure 3), variations in the pixel fraction of Dark Green are plausibly attributable to decreases in Chl-*a* and carotenoids concentrations, which is a common response to salinity (e.g., Carter and Knapp, 2001; Fozouni *et al.,* 2012a; Fozouni *et al.,* 2012b). The Chl-*b* concentration tended to decrease, but it was not significantly reduced compared to CTRL, likely due to the duration of stress and/or the limited number of observations. The decrease in carotenoids might be explained by considering that the main hormone involved in salt stress regulation is abscisic acid (Ryu and Cho, 2015), whose biosynthesis involves carotenoids as precursors (Seo and Koshiba, 2002). By contrast, leaf carotenoids would be stable in case of chlorosis symptoms triggered, for example, by N deficiency (Rustioni *et al.,* 2018). In addition, considering that reflectance spectroscopy supports the identification of chlorophylls and carotenoids (and their relative change) in grapevine leaves

(Rustioni *et al.,* 2018), image-based salt stress phenotyping might be integrated with that signal. Following this, it can reasonably be said that image-based phenotyping (namely the Dark Green colour band) is a promising phenotyping tool for tracking the early stage of salt stress. This would also be supportive for proximal and remote vineyard phenomics in a precision agriculture domain (Meggio *et al.,* 2010; Taskos *et al.,* 2015).

Nowadays, image-based and affordable phenotyping is extensively employing RGB cameras (Reynolds *et al.,* 2018; Ninomiya, 2022). Accordingly, the use of R, G and B and related indexes would be of interest in phenotyping salt stress as most of these indexes have been associated with changes in leaf pigment concentrations (see Montanaro *et al.,* 2023 and the references therein), which are sensitive to salt stress as reported by Panda *et al.* (2013) in *Oryza sativa* and Sohrabi *et al.* (2017) in grapevines. In line with this, correlative information collected in our study supports that idea, at least for some colorimetric indexes (Figure 11A). In addition, salt-induced changes of the RGB colorimetric indexes were, in most cases, linearly coupled to EC values beyond 4 dS m^{-1}, which fits with the soil ECt threshold discussed above. Particularly, it should be noted that the mean pixel value of the CI colorimetric index and R channel were able to explain a large part of EC variance when greater than ECt ($R^2 > 0.80$) (Figure 11B). Considering that the employment of RGB-based colorimetric indexes as predictors of plant/fruit traits are increasingly used as input variables of artificial neural networks (ANN), achieving a considerable improvement in their predicting capability (Picón *et al.,* 2022; Wei *et al.,* 2022), the combination of RGB-based indexes and ANN in a salt stress phenotyping context deserves future research. Moreover, as the osmotic stress promptly reduces stomatal conductance and, in turn, changes the leaf temperature (Jones *et al.,* 2002), it is advisable to combine RGB-based imaging with thermal ones also in view of its affordable low cost (Reynolds *et al.,* 2019; Ninomiya, 2022).

The present study documented that RGB-based imaging (namely the fraction of the Dark Green colour band) is a promising phenotyping tool for tracking the early stages of salt stress, easily supporting the identification of critical thresholds of soil EC. This study also pointed out the robustness of some RGB-based colorimetric indexes to serve as a proxy within affordable phenotyping of salt stress. In view of the increasing need for alternative water resources, such as saline waters for irrigation in grapevine (Martínez-Moreno *et al.,* 2022), this study contributes to identifying smart proxies potentially enabling the management of vineyard under salt stress in a digital viticulture domain.

REFERENCES

Acosta-Gamboa, L., Liu, S., Langley, E., Campbell, Z. C., Castro-Guerrero, N., Mendoza-Cózatl, D. G., & Lorence, A. (2017). Moderate to severe water limitation differentially affects the phenome and ionome of Arabidopsis. *Functional Plant Biology*, *44*(1), 94. https://doi.org/10.1071/fp16172

Amato, D., Montanaro, G., Summerer, S., Briglia, N., Attia, F., Challet, E., & Nuzzo, V. (2020). The effects of calcite silicon-mediated particle film application on leaf temperature and grape composition of Merlot (*Vitis vinifera L.*) vines under different irrigation conditions. *OENO One*, *54*(4), 1007–1020. https://doi.org/10.20870/oeno-one.2020.54.4.4020

Amorim, T. L., Santos, H. R. B., Neto, J. B., Hermínio, P. J., Silva, J. R. I., Silva, M. M. A., Simões, A. N., De Souza, E. S., & Ferreira-Silva, S. L. (2023). Resistant rootstocks mitigate ionic toxicity with beneficial effects for growth and photosynthesis in grapevine grafted plants under salinity. *Scientia Horticulturae*, *317*, 112053. https://doi.org/10.1016/j.scienta.2023.112053

Arvidsson, S., Pérez-Rodríguez, P., & Mueller-Roeber, B. (2011). A growth phenotyping pipeline for *Arabidopsis thaliana* integrating image analysis and rosette area modeling for robust quantification of genotype effects. *New Phytologist*, *191*(3), 895–907. https://doi.org/10.1111/j.1469-8137.2011.03756.x

Atieno, J., Li, Y., Langridge, P., Dowling, K., Brien, C., Berger, B., Varshney, R. K., & Sutton, T. (2017). Exploring genetic variation for salinity tolerance in chickpea using image-based phenotyping. *Scientific Reports*, *7*(1). https://doi.org/10.1038/s41598-017-01211-7

Baggett, J. P., Habibsadeh, S., Toups, H. S., Cochetel, N., Ghan, R., Robinson, M. L., Barrios-Masias, F. H., & Cramer, G. R. (2021). Is foliar Cl- concentration the cause of photosynthetic decline in grapevine during mild salinity? *OENO One*, *55*(4), 33–48. https://doi.org/10.20870/oeno-one.2021.55.4.4795

Baneh, H. D., Hassani, A., & Shaieste, F. G. (2014). Effects of salinity on leaf mineral composition and salt injury symptoms of some Iranian wild grapevine (*Vitis vinifera* L. ssp. sylvestris) genotypes. *OENO One*, *48*(4), 231. https://doi.org/10.20870/oeno-one.2014.48.4.1692

Ben-Asher, J., Tsuyuki, I., Bravdo, B., & Sagih, M. (2006). Irrigation of grapevines with saline water: I. Leaf area index, stomatal conductance, transpiration and photosynthesis. *Agricultural Water Management 83*, 13–21 https://doi.org/10.1016/j.agwat.2006.01.002

Briglia, N., Montanaro, G., Petrozza, A., Summerer, S., Cellini, F., & Nuzzo, V. (2019). Drought phenotyping in Vitis vinifera using RGB and NIR imaging. *Scientia Horticulturae*, *256*, 108555. https://doi.org/10.1016/j.scienta.2019.108555

Briglia, N., Williams, K., Wu, D., Li, Y., Tao, S., Corke, F., Montanaro, G., Petrozza, A., Amato, D., Cellini, F., Doonan, J., Yang, W., & Nuzzo, V. (2020). Image-Based assessment of drought response in grapevines. *Frontiers in Plant Science*, *11*. https://doi.org/10.3389/fpls.2020.00595

Carter, G. A., & Knapp, A. K. (2001). Leaf optical properties in higher plants: linking spectral characteristics to stress and chlorophyll concentration. *American Journal of Botany*, *88*(4), 677–684. https://doi.org/10.2307/2657068

Choné, X., Van Leeuwen, C., Dubourdieu, D., & Gaudillère, J. P. (2001). Stem Water Potential is a Sensitive Indicator of Grapevine Water Status. *Annals of Botany*, *87*(4), 477–483. https://doi.org/10.1006/anbo.2000.1361

Costa, C., Schurr, U., Loreto, F., Menesatti, P., & Carpentier, S. (2019). Plant Phenotyping Research Trends, a Science Mapping approach. *Frontiers in Plant Science*, *9*. https://doi.org/10.3389/fpls.2018.01933

Cramer, G. R., Ergül, A., Grimplet, J., Tillett, R. L., Tattersall, E. a. R., Bohlman, M. C., Vincent, D., Sonderegger, J., Evans, J. R., Osborne, C., Quilici, D. R., Schlauch, K., Schooley, D. A., & Cushman, J. C. (2006). Water and salinity stress in grapevines: early and late changes in transcript and metabolite profiles. *Functional & Integrative Genomics*, *7*(2), 111–134. https://doi.org/10.1007/s10142-006-0039-y

Dag, A., Ben-Gal, A., Goldberger, S., Yermiyahu, U., Zipori, I., Or, E., David, I., Netzer, Y., & Kerem, Z. (2015). Sodium and chloride distribution in grapevines as a function of rootstock and irrigation water salinity. *American Journal of Enology and Viticulture*, *66*(1), 80–84. https://doi.org/10.5344/ajev.2014.14019

Das, P., & Majumder, A. L. (2018). Transcriptome analysis of grapevine under salinity and identification of key genes responsible for salt tolerance. *Functional & Integrative Genomics*, *19*(1), 61–73. https://doi.org/10.1007/s10142-018-0628-6

Fozouni, M., Abbaspour, N., & Baneh, H. D. (2012a). Short term response of grapevine grown hydroponically to salinity: Mineral composition and growth parameters. *Vitis: Journal of Grapevine Research*, *51*(3), 95–101. https://doi.org/10.5073/vitis.2012.51.95-101

Fozouni, M., Abbaspour, N., & Baneh, H. D. (2012b). Leaf water potential, photosynthetic pigments and compatible solutes alterations in four grape cultivars under salinity. *Vitis: Journal of Grapevine Research*, *51*(4), 147–152. https://doi.org/10.5073/vitis.2012.51.147-152

Gadagkar, S. R., & Call, G. B. (2015). Computational tools for fitting the Hill equation to dose–response curves. *Journal of Pharmacological and Toxicological Methods*, *71*, 68–76. https://doi.org/10.1016/j.vascn.2014.08.006

Goudriaan, J., & van Laar, H. (1994). Modelling potential crop growth processes. In *Current issues in production ecology*. https://doi.org/10.1007/978-94-011-0750-1

Hairmansis, A., Berger, B., Tester, M., & Roy, S. J. (2014). Image-based phenotyping for non-destructive screening of different salinity tolerance traits in rice. *Rice*, *7*(1). https://doi.org/10.1186/s12284-014-0016-3

Hu, Y., & Schmidhalter, U. (2023). Opportunity and challenges of phenotyping plant salt tolerance. *Trends in Plant Science*, *28*(5), 552–566. https://doi.org/10.1016/j.tplants.2022.12.010

Isayenkov, S. V., & Maathuis, F. J. M. (2019). Plant salinity Stress: Many unanswered questions remain. *Frontiers in Plant Science*, *10*. https://doi.org/10.3389/fpls.2019.00080

Jones, H. G., Stoll, M., Santos, T., Sousa, C. de, Chaves, M. M., & Grant, O. M. (2002). Use of infrared thermography for monitoring stomatal closure in the field: Application to grapevine. *Journal of Experimental Botany*, 53(378), 2249–2260. https://doi.org/10.1093/jxb/erf083

Keller, M. (2010). Managing grapevines to optimise fruit development in a challenging environment: a climate change primer for viticulturists. *Australian Journal of Grape and Wine Research*, *16*, 56–69. https://doi.org/10.1111/j.1755-0238.2009.00077.x

Khan, A. A., Rao, S. A., & McNeilly, T. (2003). Assessment of salinity tolerance based upon seedling root growth response functions in maize (Zea mays L.). *Euphytica*, *131*(1), 81–89. https://doi.org/10.1023/a:1023054706489

Klukas, C., Chen, D., & Pape, J. (2014). Integrated Analysis Platform: An Open-Source information System for High-Throughput plant phenotyping. *Plant Physiology*, *165*(2), 506–518. https://doi.org/10.1104/pp.113.233932

Lichtenthaler, H. K., & Wellburn, A. R. (1983). Determinations of total carotenoids and chlorophylls *a* and *b* of leaf extracts in different solvents. *Biochemical Society Transactions*, *11*(5), 591–592. https://doi.org/10.1042/bst0110591

Maas, E. V., & Hoffman, G. J. (1977). Crop Salt Tolerance—Current Assessment. *Journal of the Irrigation and Drainage Division*, *103*(2), 115–134. https://doi.org/10.1061/jrcea4.0001137

Marín, D., Armengol, J., Carbonell-Bejerano, P., Escalona, J. M., Gramaje, D., Hernández-Montes, E., Intrigliolo, D. S., Martínez-Zapater, J. M., Medrano, H., Mirás-Avalos, J. M., Palomares-Rius, J. E., Romero-Azorín, P., Savé, R., Santesteban, L., & De Herralde, F. (2021). Challenges of viticulture adaptation to global change: tackling the issue from the roots. *Australian Journal of Grape and Wine Research*, *27*(1), 8–25. https://doi.org/10.1111/ajgw.12463

Martínez-Cob, A., Aragüés, R., & Royo, A. (1987). Salt tolerance of barley (Hordeum vulgare L.) cultivars at the germination stage: Analysis of the response functions. *Plant and Soil*, *104*(1), 53–56. https://doi.org/10.1007/bf02370624

Martínez-Moreno, A., Pérez-Álvarez, E. P., López-Urrea, R., Intrigliolo, D. S., González-Centeno, M. R., Teissèdre, P., & Gil-Muñoz, R. (2022). Is deficit irrigation with saline waters a viable alternative for winegrowers in semiarid areas? *OENO One*, *56*(1), 101–116. https://doi.org/10.20870/oeno-one.2022.56.1.4910

Martínez-Moreno, A., Pérez-Álvarez, E. P., Intrigliolo, D. S., Mirás-Avalos, J. M., López-Urrea, R., Gil-Muñoz, R., Lizama, V., García-Esparza, M. J., Álvarez, M. I., & Buesa, I. (2023). Effects of deficit irrigation with saline water on yield and grape composition of Vitis vinifera L. cv. Monastrell. Irrigation Science, 41(4), 469–485. https://doi.org/10.1007/s00271-022-00795-x

Meggio, F., Prinsi, B., Negri, A., Di Lorenzo, G. S., Lucchini, G., Pitacco, A., Failla, O., Scienza, A., Cocucci, M., & Espen, L. (2014). Biochemical and physiological responses of two grapevine rootstock genotypes to drought and salt treatments. *Australian Journal of Grape and Wine Research*, *20*(2), 310–323. https://doi.org/10.1111/ajgw.12071

Meggio, F., Zarco-Tejada, P. J., Núñez, L., Sepulcre-Cantó, G., Rebollo, M. Á. G., & Martín, P. (2010). Grape quality assessment in vineyards affected by iron deficiency chlorosis using narrow-band physiological remote sensing indices. *Remote Sensing of Environment*, *114*(9), 1968–1986. https://doi.org/10.1016/j.rse.2010.04.004

Mirás-Avalos, J. M., & Intrigliolo, D. S. (2017). Grape Composition under Abiotic Constrains: Water Stress and Salinity. *Frontiers in Plant Science*, *8*. https://doi.org/10.3389/fpls.2017.00851

Mohammadkhani, N., & Abbaspour, N. (2017). Absorption kinetics and efflux of chloride and sodium in the roots of four grape genotypes (Vitis L.) differing in salt tolerance. *Iranian Journal of Science and Technology Transaction A-science*, *42*(4), 1779–1793. https://doi.org/10.1007/s40995-017-0445-0

Montanaro, G., Briglia, N., Lopez, L., Amato, D., Panara, F., Petrozza, A., Cellini, F., & Nuzzo, V. (2022). A synthetic cytokinin primes photosynthetic and growth response in grapevine under ion-independent salinity stress. *Journal of Plant Interactions*, *17*(1), 789–800. https://doi.org/10.1080/17429145.2022.2102259

Montanaro, G., Petrozza, A., Rustioni, L., Cellini, F., & Nuzzo, V. (2023). Phenotyping key fruit quality traits in olive using RGB images and back propagation neural networks. *Plant Phenomics*, *5*. https://doi.org/10.34133/plantphenomics.0061

Munns, R., & Tester, M. (2008). Mechanisms of salinity tolerance. *Annual Review of Plant Biology*, *59*(1), 651–681. https://doi.org/10.1146/annurev.arplant.59.032607.092911

Ninomiya, S. (2022). High-throughput field crop phenotyping: current status and challenges. *Breeding Science*, *72*(1), 3–18. https://doi.org/10.1270/jsbbs.21069

OIV (2009). OIV Descriptor List for Grape Varieties and Vitis Species, 2nd ed.; OIV: Paris, France. Available on-line at https://www.oiv.int/public/medias/2274/code-2e-edition-finale.pdf

Ouyang, J., De Bei, R., & Collins, C. (2021). Assessment of canopy size using UAV-based point cloud analysis to detect the severity and spatial distribution of canopy decline. *OENO One*, *55*(1). https://doi.org/10.20870/oeno-one.2021.55.1.3078

Panagea, I., Daliakopoulos, I. N., Tsanis, I. K., & Schwilch, G. (2016). Evaluation of promising technologies for soil salinity amelioration in Timpaki (Crete): a participatory approach. *Solid Earth*, *7*(1), 177–190. https://doi.org/10.5194/se-7-177-2016

Panda, D., Ghosh D.C., & Kar M. (2013). Effect of Salt Stress on the Pigment Content and Yield of Different Rice (Oryza sativa L.) Genotypes. *International Journal of Bio-resource and Stress Management*.4(3), 431-434. https://ojs.pphouse.org/index.php/IJBSM/article/view/410

Peiró, R., Jiménez, C., Perpiñà, G., Soler, J. X., & Gisbert, C. (2020). Evaluation of the genetic diversity and root architecture under osmotic stress of common grapevine rootstocks and clones. Scientia Horticulturae, 266, 109283. https://doi.org/10.1016/j.scienta.2020.109283

Petrozza, A., Santaniello, A., Summerer, S., Di Tommaso, G., Di Tommaso, D., Paparelli, E., Piaggesi, A., Perata, P., & Cellini, F. (2014). Physiological responses to Megafol® treatments in tomato plants under drought stress: A phenomic and molecular approach. *Scientia Horticulturae*, *174*, 185–192. https://doi.org/10.1016/j.scienta.2014.05.023

Picón, A., Bereciartua-Pérez, A., Eguskiza, I., Romero-Rodriguez, J., Jimenez-Ruiz, C. J., Eggers, T., Klukas, C., & Navarra-Mestre, R. (2022). Deep convolutional neural network for damaged vegetation segmentation from RGB images based on virtual NIR-channel estimation. *Artificial Intelligence in Agriculture*, *6*, 199–210. https://doi.org/10.1016/j.aiia.2022.09.004

Poorter, H., Niinemets, Ü., Walter, A., Fiorani, F., & Schurr, U. (2010). A method to construct dose–response curves for a wide range of environmental factors and plant traits by means of a meta-analysis of phenotypic data. *Journal of Experimental Botany*, *61*(8), 2043–2055. https://doi.org/10.1093/jxb/erp358

Prior, L. D., Grieve, A., & Cullis, B. R. (1992). Sodium chloride and soil texture interactions in irrigated field grown sultana grapevines. I. Yield and fruit quality. *Australian Journal of Agricultural Research*, *43*(5), 1051. https://doi.org/10.1071/ar9921051

Reynolds, D. B., Baret, F., Welcker, C., Bostrom, A., Ball, J., Cellini, F., Lorence, A., Chawade, A., Khafif, M., Noshita, K., Mueller-Linow, M., Zhou, J., & Tardieu, F. F. (2019). What is cost-efficient phenotyping? Optimizing costs for different scenarios. *Plant Science*, *282*, 14–22. https://doi.org/10.1016/j.plantsci.2018.06.015

Rustioni, L., Grossi, D., Brancadoro, L., & Failla, O. (2018). Iron, magnesium, nitrogen and potassium deficiency symptom discrimination by reflectance spectroscopy in grapevine leaves. *Scientia Horticulturae*, *241*, 152–159. https://doi.org/10.1016/j.scienta.2018.06.097

Ryu, H., & Cho, Y. (2015). Plant hormones in salt stress tolerance. *Journal of Plant Biology*, *58*(3), 147–155. https://doi.org/10.1007/s12374-015-0103-z

Seo, M., & Koshiba, T. (2002). Complex regulation of ABA biosynthesis in plants. *Trends in Plant Science*, *7*(1), 41–48. https://doi.org/10.1016/s1360-1385(01)02187-2

Sohrabi, S., Ebadi, A., Jalali, S., & Salami, S. A. (2017). Enhanced values of various physiological traits and VvNAC1 gene expression showing better salinity stress tolerance in some grapevine cultivars as well as rootstocks. *Scientia Horticulturae*, *225*, 317–326. https://doi.org/10.1016/j.scienta.2017.06.025

Taskos, D., Koundouras, S., Stamatiadis, S., Zioziou, E., Νικολάου, N., Karakioulakis, K., & Theodorou, N. (2015). Using active canopy sensors and chlorophyll meters to estimate grapevine nitrogen status and productivity. *Precision Agriculture*, *16*(1), 77–98. https://doi.org/10.1007/s11119-014-9363-8

Upadhyay, A., Gaonkar, T., Upadhyay, A. K., Satisha, J., Shinde, M., Kadoo, N. Y., & Gupta, V. S. (2018). Global transcriptome analysis of grapevine (Vitis vinifera L.) leaves under salt stress reveals differential response at early and late stages of stress in table grape cv. Thompson Seedless. *Plant Physiology and Biochemistry*, *129*, 168–179. https://doi.org/10.1016/j.plaphy.2018.05.032

Walker, R. R., Blackmore, D. H., Clingeleffer, P. R., & Iacono, F. (1997). Effect of salinity and Ramsey rootstock on ion concentrations and carbon dioxide assimilation in leaves of drip-irrigated, field-grown grapevines (Vitis vinifera L. cv. Sultana). *Australian Journal of Grape and Wine Research*, *3*(2), 66–74. https://doi.org/10.1111/j.1755-0238.1997.tb00117.x

Weerasekara, P. C. (2017). The United Nations World Water Development Report 2017 Wastewater: the Untapped Resource. *Future of Food: Journal on Food, Agriculture and Society*, *5*(2), 80–81. http://www.futureoffoodjournal.org/index.php/journal/article/view/311

Wei, X., Wu, L., Ge, D., Yao, M., & Bai, Y. (2022). Prediction of the maturity of greenhouse grapes based on imaging technology. *Plant Phenomics*, *2022*. https://doi.org/10.34133/2022/9753427

Xue, W., Yan, J., Zhao, G., Jiang, Y., Cheng, J., Cattivelli, L., & Tondelli, A. (2017). A major QTL on chromosome 7HS controls the response of barley seedling to salt stress in the Nure × Tremois population. *BMC Genomic Data*, *18*(1). https://doi.org/10.1186/s12863-017-0545-z

Yu, R. and Kurtural, S.K. (2020). Proximal sensing of soil electrical conductivity provides a link to soil-plant water relationships and supports the identification of plant water status zones in vineyards. *Frontiers in Plant Science 11*, https://doi.org/10.3389/fpls.2020.00244.